Journal of Power Sources 195 (2010) 1441–1445

Contents lists available at ScienceDirect

Journal of Power Sources

journal homepage: www.elsevier.com/locate/jpowsour

Short communication

Rational design of novel cathode materials in solid oxide fuel cells using first-principles simulations

YongMan Choi[a,1], M.C. Lin[b,c], Meilin Liu[a,*]

[a] Center for Innovative Fuel Cell and Battery Technologies, School of Materials Science and Engineering, Georgia Institute of Technology, 771 Ferst Drive, N.W., Atlanta, GA 30332, USA
[b] Department of Chemistry, Emory University, 1515 Dickey Drive, Atlanta, GA 30322, USA
[c] Center for Interdisciplinary Molecular Science, National Chiao Tung University, Hsinchu 30010, Taiwan

ARTICLE INFO

Article history:
Received 29 May 2009
Received in revised form 8 September 2009
Accepted 9 September 2009
Available online 16 September 2009

Keywords:
Solid oxide fuel cells
First-principles calculations
ABO_3-type cathodes
Oxygen reduction
Ionic transport

ABSTRACT

The search for clean and renewable sources of energy represents one of the most vital challenges facing us today. Solid oxide fuel cells (SOFCs) are among the most promising technologies for a clean and secure energy future due to their high energy efficiency and excellent fuel flexibility (e.g., direct utilization of hydrocarbons or renewable fuels). To make SOFCs economically competitive, however, development of new materials for low-temperature operation is essential. Here we report our results on a computational study to achieve rational design of SOFC cathodes with fast oxygen reduction kinetics and rapid ionic transport. Results suggest that surface catalytic properties are strongly correlated with the bulk transport properties in several material systems with the formula of $La_{0.5}Sr_{0.5}BO_{2.75}$ (where B = Cr, Mn, Fe, or Co). The predictions seem to agree qualitatively with available experimental results on these materials. This computational screening technique may guide us to search for high-efficiency cathode materials for a new generation of SOFCs.

1. Introduction

Solid oxide fuel cells (SOFOs) have attracted considerable attention due to their high energy efficiency and excellent fuel flexibility (e.g., the potential for direct utilization of hydrocarbons, coal gas, biomass, and other renewable fuels [1,2]). To realize these unique advantages over other types of fuel cells, however, several critical challenges must be overcome, including anode deactivation by coking and contaminates (e.g., sulfur) poisoning, cathode degradation by chromia poisoning, and high cost for broad commercialization [3]. One effective approach to cost reduction is to reduce the operating temperature of SOFCs. At sufficiently low operating temperatures, the interconnect, heat exchangers, and other structural components can be fabricated from much less expensive materials. Further, as the operating temperature is reduced, many technical difficulties will find easy solutions, system reliability and operational life increase, and so is the possibility of using SOFCs for a wider range of applications. It is noted, however, that the interfacial polarization resistances increase rapidly as the operating temperature is reduced, especially the resistances to oxygen reduction on the cathode [4], implying that the creation of novel cathode materials with high catalytic activity toward oxygen reduction at low temperatures represents a critical step toward the development of low-cost SOFCs [5]. To reduce cathodic polarization, mixed ionic–electronic conductors (MIECs) such as $(La_{1-x}Sr_x)(B_{1-y}B'_y)O_{3-\delta}$ (B or B′ = Mn, Co, or Fe) have been widely used as cathode for SOFCs. It has been reported that $LaCoO_3$-based cathode materials exhibit better performance than $LaMnO_3$-based ones [6], although the detailed mechanisms of oxygen reduction on these materials are still not clear. Recently, density functional theory (DFT) calculations have been used to examine the energetics for the elementary steps involved in oxygen reduction on $LaMnO_3$-based cathodes ($LaMnO_3$ and $La_{0.5}Sr_{0.5}MnO_{2.75}$) [7–9], including adsorption, dissociation, incorporation, and diffusion to triple-phase boundaries (TPBs) where a cathode, an electrolyte, and oxygen species meet. In addition to the kinetics of the oxygen reduction reaction on cathode surfaces, transport of oxygen ions to/away from the surface active sites plays an important role in rational design of novel cathode materials for SOFCs [10,11]. Secondary ion mass spectrometry (SIMS) [10,12,13] is considered one of the most reliable experimental techniques for determination of oxygen ion diffusivity and catalytic properties (e.g., surface oxygen exchange coefficient) of MIEC cathode materials. Further, a series of atomistic simulations [14–17] have also been used to predict ionic transport through ABO_3-type materials. In this study, we report our results on a theoretical prediction, on the basis of first-principles

* Corresponding author. Tel.: +1 404 894 6114; fax: +1 404 894 9140.
E-mail address: meilin.liu@mse.gatech.edu (M. Liu).
[1] Present address: Chemistry Department, Brookhaven National Laboratory, Upton, NY 11973, USA.

0378-7753/$ – see front matter © 2009 Published by Elsevier B.V.
doi:10.1016/j.jpowsour.2009.09.017

methods, of both surface reactions and bulk diffusion in Sr-doped $LaBO_3$-based cathode materials (B = Cr, Mn, Fe, or Co). In particular, we have investigated how ionic diffusion through bulk cathodes and surface interactions between oxygen species at their surfaces influence the efficiency of the cathode performance in an SOFC, providing important insight into rational design of high-performance cathode materials for SOFCs.

2. Computational

For electronic-structure calculations, the Vienna *ab initio* simulation package (VASP) [18,19] was used with projector augmented wave (PAW) potentials [20]. La, Sr, Cr, Mn, Fe, Co, and O atoms were described by 11 ($5s^2 5p^6 5d^1 6s^2$), 10 ($4s^2 4p^6 5s^2$), 6 ($4s^1 3d^5$), 7 ($4s^1 3d^6$), 8 ($4s^1 3d^7$), 9 ($4s^1 3d^8$), and 6 ($2s^2 2p^4$) valence electrons, respectively, while Ce, Pr, Nd, Pm, and Sm atoms were described by 12 ($5s^2 5p^6 4f^1 5d^1 6s^2$), 11 ($5s^2 5p^6 5d^1 6s^2$), 11 ($5s^2 5p^6 5d^1 6s^2$), 11 ($5s^2 5p^6 5d^1 6s^2$), 11 ($5s^2 5p^6 5d^1 6s^2$), and 10 ($5s^2 5p^6 5d^1 6s^1$), respectively. The Perdew–Wang (PW91) exchange-correlation functional [21] was applied. All calculations were performed using the electron spin polarization with a 400 eV kinetic energy cutoff for a plane wave basis set and a Monkhorst–Pack [22] mesh with $(4 \times 4 \times 4)$ *k*-points. The Jahn–Teller distortion may not be critical under SOFC operating conditions (above 500 °C at ambient air) [23,24] since $LaMnO_3$-based materials have a cubic crystal structure. In addition, Predith and Ceder [25] successfully demonstrated oxygen ionic transport phenomena through cubic perovskite-structure ABO_3 (A = Ba or Sr and B = Mn, Fe, Co or Ru) using DFT calculations. Thus, we applied the *Pm*3*m* crystal structure to construct La-based surface models similar to previous studies [26–30] on $LaMnO_3$-based materials. Regarding the magnetic properties, only FM states were applied in this study because ferromagnetic (FM) configurations are more stable than antiferromagnetic (AFM) configurations with a difference in energy of 0.02–0.25 eV, depending on B cations.

3. Results and discussion

3.1. Prediction of bulk-diffusion barriers

The validity of the surface models used in this study was confirmed by comparing the predicted diffusion barriers with those determined from experimental SIMS results. All bulk-diffusion calculations were carried out on Sr-doped $LaBO_3$(1 1 0) since it is reported [15] that ionic diffusion may occur most likely in the (1 1 0) direction. Because the defect structures of $(La_{1-x}Sr_x)(B_{1-y}B'_y)O_{3-\delta}$ (B or B′ = Mn, Co, or Fe) depend strongly on temperature and partial pressure of oxygen [31,32], we constructed a simplified surface model with a stoichiometry of $La_{0.5}Sr_{0.5}BO_{2.75}$. Four surface models, $La_{0.5}Sr_{0.5}CrO_{2.75}$ (**LSCr50**), $La_{0.5}Sr_{0.5}MnO_{2.75}$ (**LSM50**), $La_{0.5}Sr_{0.5}FeO_{2.75}$ (**LSF50**), and $La_{0.5}Sr_{0.5}CoO_{2.75}$ (**LSC50**), were constructed according to the following defect reaction:

$$2SrO + 2La_{La}^{x} + O_{O}^{x} \rightarrow 2Sr'_{La} + V_O^{\bullet\bullet} + La_2O_3,$$

where La_{La}^{x}, O_{O}^{x}, Sr'_{La}, and $V_O^{\bullet\bullet}$ are a La cation at a regular La site, an oxygen ion at a regular oxygen site in the bulk phase, a Sr cation at a La site, and an oxygen vacancy, respectively. Recently, Pornprasertshk et al. [33] reported that diffusion barriers of oxygen ions through bulk phases are influenced by locations of oxygen vacancies and neighboring ions, leading to enormous number of possible configurations. To minimize the number of possible surface models and to examine the effect of oxygen vacancies on the

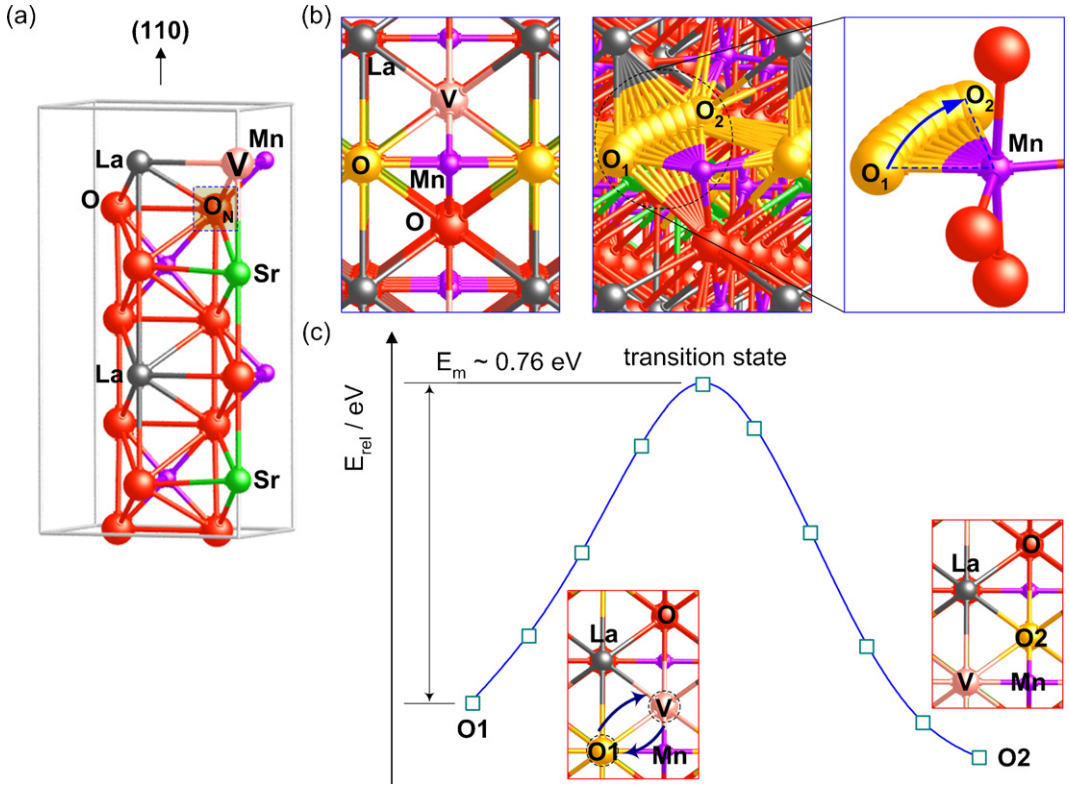

Fig. 1. Schematic of a surface model for the examination of ionic diffusion through bulk phases. (a) The $La_{0.5}Sr_{0.5}MnO_{2.75}$(1 1 0) surface model. (b) Top and side views of a bulk $La_{0.5}Sr_{0.5}MnO_{2.75}$(1 1 0) structure before and after ionic conduction. The supercell used in this study contains a total of 19 ions (2 La, 2 Sr, 4 B, and 11 O ions) and an oxygen vacancy. V and O_N denote an oxygen vacancy and the nearest neighboring oxygen to V, respectively. (c) Trajectory of oxygen ion conduction through $La_{0.5}Sr_{0.5}MnO_{2.75}$(1 1 0). **O1** and **O2** denote initial and final states of oxygen ion conduction. For clarity, oxygen ions involving bulk diffusion are presented in yellow. (For interpretation of the references to colour in this figure legend, the reader is referred to the web version of the article.)

Table 1
Predicted properties and diffusion barriers of oxygen ionic conduction through $La_{0.5}Sr_{0.5}BO_{2.75}$ (B = Cr, Mn, Fe, or Co) at the GGA-PW91 level.

	$La_{0.5}Sr_{0.5}CrO_{2.75}$	$La_{0.5}Sr_{0.5}MnO_{2.75}$	$La_{0.5}Sr_{0.5}FeO_{2.75}$	$La_{0.5}Sr_{0.5}CoO_{2.75}$
Bulk diffusion				
E_m	0.75	0.76	0.42	0.38
$E_{O\text{-vac}}$	3.56	3.25	2.41	1.49
$E_{a,calc.}$	4.31	4.01	2.83	1.87
$E_{a,expt.}$ [a]	–	3.76 ± 0.33	–	1.41 ± 0.02
Surface interactions				
ΔE_{ads}, superoxo-	−1.86	−1.37	−1.07	−0.82
ΔE_{ads}, peroxo-	−2.03	−1.20	−0.78	−0.09
ΔE_{ads}, mean	−1.95	−1.28	−0.92	−0.45

[a] From Refs. [12,13].

O_2-cathode interactions, we located an oxygen vacancy on the top layer, as shown in Fig. 1a. Furthermore, similar to the previous studies [33,34], we assumed that the diffusion barrier heights depend strongly on the nearest oxygen ion site to an oxygen vacancy. The ionic conductivity (D) can be predicted using transition state theory (TST) [35] according to

$$D = D_0 \exp\left(-\frac{E_a}{k_B T}\right),$$

where D_0, E_a, k_B, and T denote a pre-exponential factor, an diffusion barrier in eV at 0 K, Boltzmann's constant, and temperature in K, respectively. Diffusion barrier E_a can further be described [36] by

$$E_a = E_m + E_{O\text{-vac}},$$

where E_m and $E_{O\text{-vac}}$ are a migration barrier of an oxygen ion through bulk phases and an oxygen-vacancy formation energy, respectively. On the basis of the previous work for predicting the migration barriers for perovskite-type materials by means of atom-

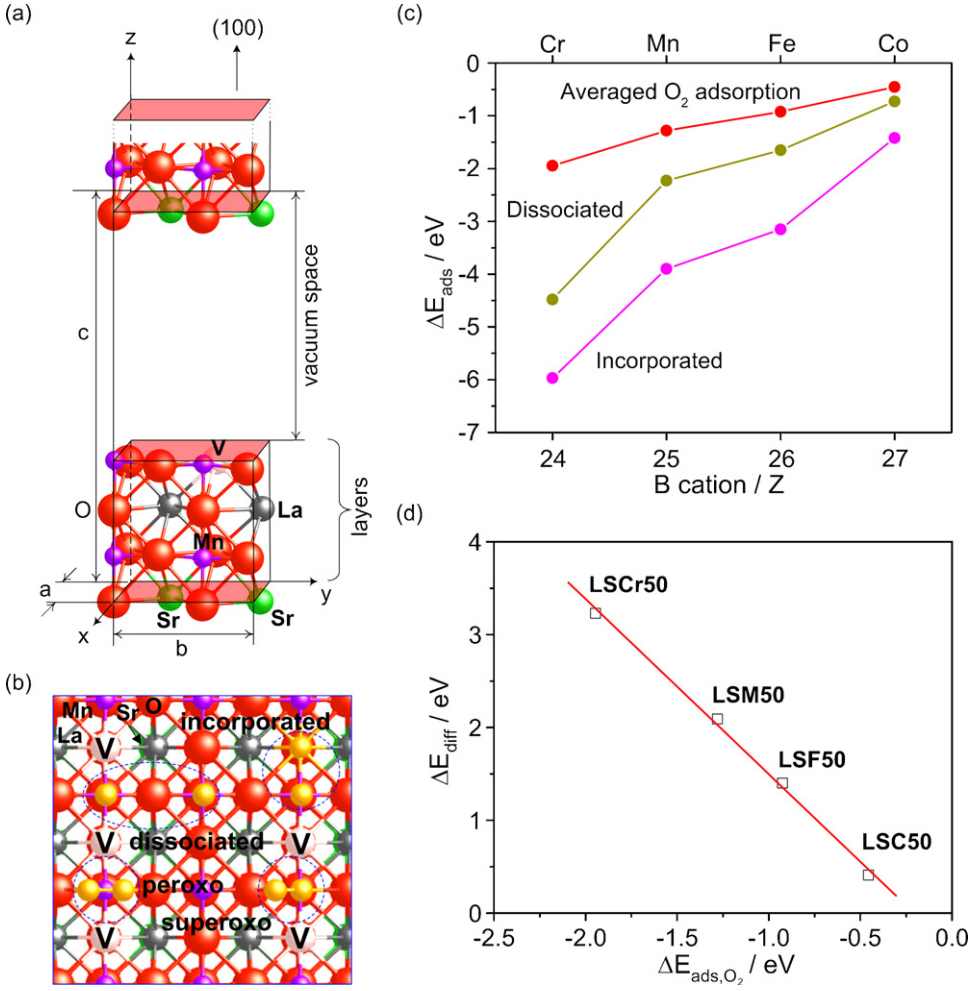

Fig. 2. Illustration of surface oxygen species on the LSM50(1 0 0) surface. The colors illustrating atoms are the same as those used in Fig. 1. (a) A representative surface model with four layers for the interactions between oxygen species and $La_{0.5}Sr_{0.5}MnO_{2.75}$. (b) The species in dashed circles are surface oxygen species formed via adsorption or incorporation into oxygen vacancies. V denotes an oxygen vacancy. (c) Adsorption energies of surface oxygen species versus B cations. Averaged O_2 adsorption corresponds to averaged adsorption energies of superoxo- and peroxo-like species. "Dissociated" denotes the adsorption energies of two dissociated oxygen species, while and "Incorporated" is that one of dissociated oxygen species is incorporated into an oxygen vacancy. (d) A correlation between surface diffusion barriers of adsorbed O species on B cations (ΔE_{diff}) and averaged O_2 adsorption energies on four Sr-doped $LaBO_{2.75}$ surfaces ($\Delta E_{ads,O_2}$).

istic modeling techniques [15–17], we predicted barrier heights of oxygen ion migration using the nudged elastic band (NEB) method [37]. Shown in Fig. 1b are the initial and final sites of oxygen ions in the **LSM50** surface model, clearly illustrating a curved trajectory of the oxygen vacancies from position **O1** to position **O2**. The non-straight trajectory is in agreement with previous studies [14], where they predicted a 0.86 eV migration barrier of oxygen ions through the $LaMnO_3$ bulk using atomistic modeling techniques. However, it is not straightforward to compare with our results because dopant Sr^{2+} cations influence the barrier height. In addition, as Islam discussed [15], because the predicted value from atomistic modeling is from only oxygen-vacancy migrations, they are much lower than those determined from SIMS data—De Souza and Kilner [12,13] reported that an experimental activation energy of **LSM50** from the SIMS technique is 3.76 ± 0.33 eV. In order to predict its diffusion barrier, we estimated $E_{\text{O-vac}}$ ($La_{0.5}Sr_{0.5}BO_3 \rightarrow La_{0.5}Sr_{0.5}BO_{2.75} + V_O^{\bullet\bullet} + (1/2)O_{2(g)}$) according to

$$E_{\text{O-vac}} = E[La_{0.5}Sr_{0.5}BO_{2.75}] + \tfrac{1}{2}E[O_2] - E[La_{0.5}Sr_{0.5}BO_3],$$

where $La_{0.5}Sr_{0.5}BO_3$ and $La_{0.5}Sr_{0.5B}MO_{2.75}$ denote Sr-doped La-based cathodes without and with an oxygen vacancy ($V_O^{\bullet\bullet}$), respectively [38], while $E[O_2]$ is the predicted electronic energy of triplet O_2 in a 10 Å cubic box. As shown in Fig. 1c, the calculated migration energy of **LSM50** is 0.76 eV. If predicted oxygen-vacancy formation energy of 3.25 eV is added, it is closer to the experimental result (4.01 eV in Table 1). Thus, we assumed that our computational approach using the surface model (see Fig. 1a) may be sufficient enough for further DFT calculations. After replacing Mn with Cr, Fe, or Co, we carried out similar predictions as summarized in Table 1. For **LSC50**, a predicted E_a of 1.87 eV is slightly higher than that determined from experiment (1.41 ± 0.02 eV) [12,13]. Our prediction clearly shows that **LSC50** has the lowest diffusion barrier for oxygen ion transport (**LSC50** > **LSF50** > **LSM50** > **LSCr50**), suggesting that LSC-based MIEC cathodes allows for faster ionic transport than other three materials.

3.2. Interactions between oxygen species and $La_{0.5}Sr_{0.5}BO_{2.75}$

As mentioned earlier, understanding the mechanisms of the interactions between oxygen species and MIEC cathode surfaces are crucial to achieving rational design of high-performance cathode materials for SOFCs. As Greeley et al. [39] described on the basis of the Sabatier principle [40], the bond strength between intermediate species and surfaces plays a significant role in understanding catalytic activity of surfaces. To examine the interactions of oxygen species with four MIEC cathode materials, we constructed the (1 0 0) surface for each, which is energetically the most stable one among the low-index (1 1 0), (1 1 0), and (1 0 0) surfaces [8,23]. Then, we carried out 2D slab-model calculations based on the four-layer (1 0 0) surfaces to examine O_2–$La_{0.5}Sr_{0.5}BO_{2.75}$ interactions, as shown in Fig. 2a. A vacuum space with ~24 Å in the perpendicular direction to the surface was used to guarantee no interactions between slabs. All surface calculations were performed by relaxing the top two layers while fixing the bottom two layers to the estimated bulk parameters. The relative energies for the O_2-surface interactions are calculated according to $\Delta E_{\text{ads}} = E_P - E_R$, where E_P and E_R are the calculated energies of products and reactants, respectively. Illustrated in Fig. 2b are energetically the most plausible configurations, including molecular adsorption, dissociation, and incorporation into an oxygen vacancy. Table 1 compiles the adsorption energies of energetically stable configurations for kinetic and mechanistic studies [9]. Further, Fig. 2c clearly shows that the adsorption energies of adsorbed species (e.g., molecular adsorption, dissociation, and incorporation processes) are well correlated with the B cations in the four Sr-doped $LaBO_3$ cathodes. This means that the bond strength between B cation and O atom may be a crucial indication of catalytic activity toward oxygen reduction for charge transfer from d orbital of B cations to 2p orbital of molecular oxygen [7]. Cr-based MIEC cathodes have the strongest bond with adsorbed oxygen species. However, regarding surface exchange coefficients associated with a surface catalytic activity toward oxygen reduction, **LSC50** has a much faster O_2 kinetics than **LSM50** [12,13]. Although one has to take into account other parameters (e.g., the concentrations of oxygen vacancies, electrons, and electron holes) [41] to estimate surface oxygen exchange coefficients, the trend shown in Fig. 2c seems to suggest that the adsorption-energy calculations are reasonably related to the catalytic activity toward oxygen reduction. Compared with the parameters determined from SIMS [12,13], our DFT calculations verify that LSC-based MIEC cathodes have the highest catalytic activity. Furthermore, Fig. 2d manifests that the surface diffusion of adsorbed oxygen species after dissociation also have a strong relevance to the B cations, indicating that the bond strength between surfaces and oxygen species becomes weaker as Z increases. This may mean that the adsorbed oxygen species or oxygen ions after dissociation/incorporation processes, respectively, on **LSC50** can more easily diffuse on the surface or to the TPB compared to others. In addition, on the basis of the estimation of the bulk-diffusion barriers (E_a) of oxygen ions through the MIEC bulk phases and the adsorption energies ($\Delta E_{\text{ads},O_2}$), we examined their correlation as shown in Fig. 3. The four cathodes materials ($La_{0.5}Sr_{0.5}CrO_{2.75}$, **LSCr50**; $La_{0.5}Sr_{0.5}MnO_{2.75}$, **LSM50**; $La_{0.5}Sr_{0.5}FeO_{2.75}$, **LSF50**; $La_{0.5}Sr_{0.5}CoO_{2.75}$, **LSC50**) show a very good correlation with a slight deviation of **LSM50**.

We then examined the effect of A cation substitution by replacing La with Ce, Pr, Nd, Pm, and Sm ($Ce_{0.5}Sr_{0.5}MnO_{2.75}$, **CeSM50**; $Pr_{0.5}Sr_{0.5}MnO_{2.75}$, **PrSM50**; $Nd_{0.5}Sr_{0.5}MnO_{2.75}$, **NdSM50**; $Pm_{0.5}Sr_{0.5}MnO_{2.75}$, **PmSM50**; $Sm_{0.5}Sr_{0.5}MnO_{2.75}$, **SSM50**, respectively). Interestingly, only **SSM50** have a much closer character to **LSC50**, implying that Sm may play a role in exhibiting a higher catalytic activity toward oxygen reduction and a lower diffusion barrier. Our further examination of $Sm_{0.5}Sr_{0.5}CoO_{2.75}$ (**SSC50**) and $Sm_{0.5}Sr_{0.5}FeO_{2.75}$ (**SSF50**) verifies the Sm effect (see Fig. 3). It is noted that our prediction of the activation barrier of **SSC50** is in excellent agreement with the experimental value (1.1 eV vs. 0.9 eV) [42]. Thus, Fig. 3 manifests that the adsorption energies of oxygen species have a strong correlation with the diffusion barriers of oxygen ion transport. Comparison with cathode materials that are

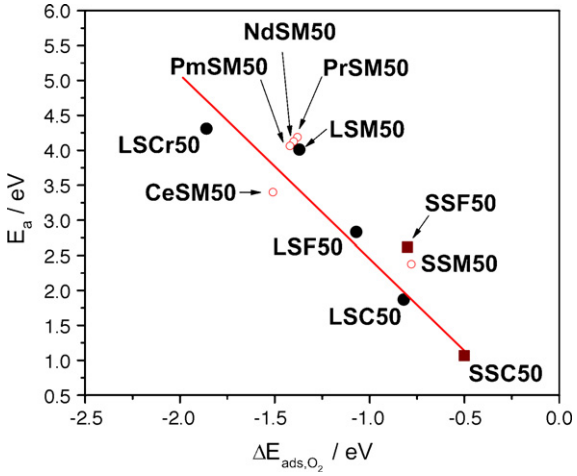

Fig. 3. Comparison of adsorption energies versus diffusion barriers of oxygen ions through the MIEC bulk phases. E_a denotes the diffusion barriers of oxygen ion transport through the bulk MIEC phases, while $\Delta E_{\text{ads},O_2}$ is the averaged adsorption energies of superoxo- and peroxo-like species on B cations. The linear line in red was obtained from **LSCr50**, **LSM50**, **LSF50**, and **LSC50**.

known catalytically active at low temperatures (LSC and SSC) suggests that tailoring novel cathode materials must also consider the need for a weak binding between a surface and oxygen species with a low O-diffusion barrier, although other factors (such as thermal mismatch with the electrolyte materials) have to be considered as well. We will extend our simulations to more realistic surface models $(A_{1-x}A'_x)(B_{1-y}B'_y)O_{3-\delta}$ (i.e., A = La or Sm, A′ = Sr, B = Co, B′ = Fe or Mn) to predict the effect of defects and other relevant conditions on surface catalytic and ionic transport properties.

4. Conclusion

Our comparative study demonstrated that LSC is the most efficient cathode material among the four considered due to its fast diffusion on surfaces and through the bulk phases, qualitatively in agreement with experimental results derived from the performances of SOFCs based on the materials [6]. Prediction of diffusion barriers and adsorption energies after dissociation/incorporation may provide vital information for rational design of better ABO_3-type cathode materials for SOFCs. Thus, DFT calculations can be a useful tool to search for high-performance cathode materials. Further, DFT based results may be combined with kinetic Monte Carlo (KMC) methods to simulate electrochemical behavior of cathode materials under SOFC operation conditions [33,43], which can be verified by electrochemical measurements.

Acknowledgements

This work was supported by DOE-NETL University Coal Program (Grant No. DE-FG26-06NT42735) and DOE Basic Energy Science (Grant No. DE-FG02-06ER15837). The authors acknowledge the use of CPUs from National Center for High-performance Computing, Taiwan. M.C.L. also wants to acknowledge the supports from the MOE ATP program, Taiwan Semiconductor Manufacturing Co. for the TSMC Distinguished Professorship and Taiwan National Science Council for the Distinguished Visiting Professorship at the Center for Interdisciplinary Molecular Science, National Chiao Tung University, Hsinchu, Taiwan.

References

[1] N.Q. Minh, T. Takahashi, Science and Technology of Ceramic Fuel Cells, Elsevier, Amsterdam, 1995.
[2] S.C. Singhal, K. Kendall, High-temperature Solid Oxide Fuel Cells: Fundamentals, Design and Applications, Elsevier Science, 2003.
[3] Y. Choi, D.S. Mebane, J.-H. Wang, M. Liu, Top. Catal. 46 (2007) 386–401.
[4] C. Xia, M. Liu, Adv. Mater. 14 (2002) 521–523.
[5] B.C.H. Steele, A. Heinzel, Nature 414 (2001) 345–352.
[6] Y. Takeda, R. Kanno, M. Noda, Y. Tomida, O. Yamamoto, J. Electrochem. Soc. 134 (1987) 2656–2661.
[7] Y. Choi, M.C. Lin, M. Liu, Angew. Chem. Int. Ed. 46 (2007) 7214–7219.
[8] Y. Choi, D.S. Mebane, M.C. Lin, M. Liu, Chem. Mater. 19 (2007) 1690–1699.
[9] Y. Choi, M.E. Lynch, M.C. Lin, M. Liu, J. Phys. Chem. C 113 (2009) 7290–7297.
[10] J.A. Kilner, Faraday Discuss. 134 (2007) 9–15.
[11] J. Maier, Solid State Ionics 112 (1998) 197–228.
[12] R.A. De Souza, J.A. Kilner, Solid State Ionics 106 (1998) 175–187.
[13] R.A. De Souza, J.A. Kilner, Solid State Ionics 126 (1999) 153–161.
[14] M. Cherry, M.S. Islam, C.R.A. Catlow, J. Solid State Chem. 118 (1995) 125–132.
[15] M.S. Islam, J. Mater. Chem. 10 (2000) 1027–1038.
[16] M.S. Islam, Solid State Ionics 154–155 (2002) 75–85.
[17] C. Tealdi, L. Malavasi, C.A.J. Fisher, M.S. Islam, J. Phys. Chem. B 110 (2006) 5395–5402.
[18] G. Kresse, J. Hafner, Phys. Rev. B 47 (1993) 558–561.
[19] G. Kresse, J. Furthmüller, Phys. Rev. B 54 (1996) 11169–11186.
[20] P.E. Blöchl, Phys. Rev. B 50 (1994) 17953–17979.
[21] J.P. Perdew, Y. Wang, Phys. Rev. B 45 (1992) 13244–13249.
[22] H.J. Monkhorst, J.D. Pack, Phys. Rev. B 13 (1976) 5188–5192.
[23] R.A. Evarestov, E.A. Kotomin, Y.A. Mastrikov, D. Gryaznov, E. Heifets, J. Maier, Phys. Rev. B 72 (2005) 214411.
[24] Y.A. Mastrikov, E. Heifets, E.A. Kotomin, J. Maier, Surf. Sci. 603 (2009) 326–335.
[25] A. Predith, G. Ceder, in: E.D. Wachsman, W. Weppner, E. Traversa, M. Liu, P. Vanysek, N. Yamazoe (Eds.), Proceedings of the Symposium on Solid-state Ionic Devices: Solid-state Ionic Devices II: Ceramic Sensors, vol. 2000-32, Electrochemical Society, Pennington, NJ, 2001, pp. 182–189.
[26] N.N. Kovaleva, J.L. Gavartin, A.L. Shluger, A.V. Boris, A.M. Stoneham, J. Exp. Theor. Phys. 94 (2002) 178–190.
[27] P. Ravindran, A. Kjekshus, H. Fjellvag, A. Delin, O. Eriksson, Phys. Rev. B 65 (2002) 064445.
[28] R.A. Evarestov, E.A. Kotomin, E. Heifets, J. Maier, G. Borstel, Solid State Commun. 127 (2003) 367–371.
[29] R.A. Evarestov, E.A. Kotomin, D. Fuks, J. Felsteiner, J. Maier, Appl. Surf. Sci. 238 (2004) 457–463.
[30] E.A. Kotomin, Y.A. Mastrikov, E. Heifets, J. Maier, Phys. Chem. Chem. Phys. 10 (2008) 4644–4649.
[31] J.H. Kuo, H.U. Anderson, D.M. Sparlin, J. Solid State Chem. 83 (1989) 52–60.
[32] J. Mizusaki, N. Mori, H. Takai, Y. Yonemura, H. Minamiue, H. Tagawa, M. Dokiya, H. Inaba, K. Naraya, T. Sasamoto, T. Hashimoto, Solid State Ionics 129 (2000) 163–177.
[33] R. Pornprasertsuk, J. Cheng, H. Huang, F.B. Prinz, Solid State Ionics 178 (2007) 195–205.
[34] F. Shimojo, H. Okazaki, J. Phys. Soc. Jpn. 61 (1992) 4106–4118.
[35] K.J. Laidler, Chemical Kinetics, 3rd ed., Benjamin Cummings, Massachusetts, 1997.
[36] D.A. Andersson, S.I. Simak, N.V. Skorodumova, I.A. Abrikosov, B. Johansson, Proc. Natl. Acad. Sci. U.S.A. 103 (2006) 3518–3521.
[37] G. Henkelman, B.P. Uberuaga, H. Jónsson, J. Chem. Phys. 113 (2000) 9901–9904.
[38] Y. Jiang, J.B. Adams, M.V. Schilfgaarde, J. Chem. Phys. 123 (2005) 064701.
[39] J. Greeley, T.F. Jaramillo, J. Bonde, I. Chorkendorff, J.K. Nørskov, Nat. Mater. 5 (2005) 909–913.
[40] P. Sabatier, Deutschen Chem. Gesellschaft 44 (1911) 1984–2001.
[41] R.A. De Souza, Phys. Chem. Chem. Phys. 8 (2006) 890–897.
[42] I.C. Fullarton, J.A. Kilner, B.C.H. Steele, P.H. Middleton, in: T.A. Ramanarayanan, W.L. Worrell, H.L. Tuller (Eds.), Proceedings of the 2nd International Symposium on Ionic and Mixed Conducting Ceramics, vol. 94-12, Electrochemical Society, Pennington, NJ, 1994, pp. 9–26.
[43] R. Pornprasertsuk, P. Ramanarayanan, C.B. Musgrave, F.B. Prinz, J. Appl. Phys. 98 (2005) 103513.